Physiol Genomics 25: 364–374, 2006.
First published March 22, 2006; doi:10.1152/physiolgenomics.00013.2006.

Transcriptome analysis of the ischemia-reperfused remodeling myocardium: temporal changes in inflammation and extracellular matrix

Sashwati Roy,[1] Savita Khanna,[1] Donald E. Kuhn,[1] Cameron Rink,[1] Willis T. Williams,[1] Jay L. Zweier,[2] and Chandan K. Sen[1]

Laboratory of Molecular Medicine, [1]Department of Surgery and [2]Department of Internal Medicine, Davis Heart and Lung Research Institute, The Ohio State University Medical Center, Columbus, Ohio

Submitted 27 January 2006; accepted in final form 3 March 2006

Roy, Sashwati, Savita Khanna, Donald E. Kuhn, Cameron Rink, Willis T. Williams, Jay L. Zweier, and Chandan K. Sen. Transcriptome analysis of the ischemia-reperfused remodeling myocardium: temporal changes in inflammation and extracellular matrix. *Physiol Genomics* 25: 364–374, 2006. First published March 22, 2006; doi:10.1152/physiolgenomics.00013.2006.—cDNA microarray analysis was performed to screen 15,000 genes and expressed sequence tags (ESTs) to identify changes in the ischemia-reperfused (I-R) rat myocardial transcriptome in the early (*day 2*) and late (*day 7*) inflammatory phases of acute myocardial infarction. Lists of candidate genes that were affected by I-R transiently (2 or 7 days only) or on a more sustained basis (2 and 7 days) were derived. The candidate genes represented three major functional categories: extracellular matrix, apoptosis, and inflammation. To expand on the findings from microarray studies that dealt with the two above-mentioned time points, tissues collected from *days 0*, *0.25*, *2*, *3*, *5*, and *7* after reperfusion were examined. Acute myocardial infarction resulted in upregulation of IL-6 and IL-18. Genes encoding extracellular matrix proteins such as types I and III collagen were upregulated in *day 2*, and that response progressively grew stronger until *day 7* after I-R. Comparable response kinetics was exhibited by the candidate genes of the apoptosis category. Caspases-2, -3, and -8 were induced in response to acute infarction. Compared with the myocardial tissue from the sham-operated rats, tissue collected from the infarct region stained heavily positive for the presence of active caspase-3. Laser microdissection and pressure catapulting technology was applied to harvest infarct and adjacent noninfarct control tissue from a microscopically defined region in the rat myocardium. Taken together, this work presents the first evidence gained from the use of DNA microarrays to understand the molecular mechanisms implicated in the early and late inflammatory phases of the I-R heart.

heart; oxygen; perceived hyperoxia; wound healing

AN ACUTE MYOCARDIAL INFARCTION induces ventricular remodeling, a process that can influence ventricular functions and survival outcomes (22). Ventricular remodeling is directly implicated in postinfarction development of ventricular dilatation, a predictive sign of future congestive heart failure. Time-dependent changes in ventricular architecture occur in the infarcted and noninfarcted regions, resulting in hypertrophy of the viable regions of the affected site (6). Cardiac remodeling after myocardial infarction depends on cellular responses, characterized by hypertrophy of myocytes and hyperplasia of interstitial fibroblasts (18). Animals that survive with large transmural infarctions develop heart failure without another ischemic event, as is typically seen in humans. A rat model of myocardial infarction has been extensively studied to understand the functional, structural, and molecular changes associated with clinical ischemic heart disease (23, 33). Substantial alterations in gene expression are needed to afford such profound changes within cells of the remodeling myocardium (33).

Current treatment of myocardial infarction is directed to restore blood flow to the ischemic region by thrombolysis, coronary artery bypass surgery, or percutaneous transluminal coronary angioplasty. Depending on the degree of success of the therapeutic intervention, the area at risk remains either hypoxic or is fully salvaged. When the area at risk remains hypoxic, the myocardial tissue loses its contractile function and becomes necrotic, leading to the initiation of a wound-healing process (3). This situation is experimentally modeled using the permanent ligation of coronary artery approach (33). In contrast, when blood flow through the myocardium is reestablished in time, hibernating myocardial tissue may regain its function but may also experience additional damage due to the reperfusion process itself. It is well known that reoxygenation induces free radical injury. Recently, we have demonstrated that reoxygenation may also trigger cardiac remodeling by inducing the differentiation of cardiac fibroblasts to myofibroblasts (28–30, 32). A comprehensive understanding of the myocardial biology of the infarction-affected site warrants a global approach directed toward analyzing the fundamental mechanisms as a function of time. To that end, the cDNA microarray technology has been productively employed to query 4,000+ genes in response to permanent partial ligation of the coronary artery (33). The ischemia-reperfused myocardium, however, has not been subjected to such comprehensive analysis. In this study, we employed a high-density cDNA microarray analysis approach to screen 15,000 genes and expressed sequence tags (ESTs) in the rat myocardium. The goal was to examine temporal changes in the myocardial transcriptome in response to acute ischemia-reperfusion.

MATERIALS AND METHODS

Survival Model for Coronary Artery Occlusion and Reperfusion

Sprague-Dawley rats weighing 500–550 g were subjected to ischemia-reperfusion of the heart as described previously (30). Parallel groups of rats were used as sham-operated controls. The studies were approved by the Institutional Laboratory Animal Care and Use Committee of The Ohio State University. Rats were anesthetized, intubated, and mechanically ventilated on a positive pressure respirator with room air. The body temperature was maintained at 36–37°C with a heated small-animal operating table. A left thoracotomy was performed via the fifth intercostal space to expose the heart. A 30-min

Article published online before print. See web site for date of publication (http://physiolgenomics.physiology.org).

Address for reprint requests and other correspondence: C. K. Sen, Davis Heart & Lung Research Institute, 473 W. 12th Ave., Columbus, OH 43210 (e-mail: Chandan.Sen@osumc.edu).

occlusion of left anterior descending coronary artery (LAD) was followed by reperfusion. Laser Doppler flow measurement was used to verify ischemia and reperfusion (I-R). On successful reperfusion, the thorax was closed, and negative thoracic pressure was reestablished for survival. The rats were killed 6 h to 7 days after reperfusion. For tissue harvesting, the infarcted I-R area was visualized under a dissecting microscope. Tissue samples were collected from the infarction (I-R) site. For control, tissues were collected from a location corresponding to the I-R sites in sham-operated rats. These rats were exposed to all surgical procedures except I-R.

GeneChip Probe Array Analysis

To identify sets of I-R-induced cardiac remodeling genes, we utilized the GeneChip approach (27, 30, 31). The total RNA was extracted from heart of 2- and 7-day I-R or sham tissue samples using Trizol (Gibco BRL) (29, 30). A further cleanup of RNA was performed using the RNeasy Kit (Qiagen). Quality of RNA was checked using the Agilent 2100 Bioanalyzer (29) Targets were prepared for microarray hybridization according to previously described protocols (27, 30, 31). To assess quality of hybridization, the samples were hybridized for 16 h at 45°C to GeneChip test arrays. Satisfactory samples were hybridized to the Rat Genome arrays (U230A) for the screening of >15,000 genes and ESTs. An EST is a short subsequence of a transcribed protein-coding or non-protein-coding DNA sequence. It was originally intended as a way to identify gene transcripts but has since been instrumental in gene discovery and sequence determination. An EST is produced by one-shot sequencing of a cloned mRNA, and the resulting sequence is a relatively low-quality fragment whose length is limited by current technology to ~500–800 nucleotides. ESTs are a useful resource for designing probes for DNA microarrays used to determine gene expression. The arrays were washed, stained with streptavidin-phycoerythrin, and then scanned with the GeneArray scanner (Affymetrix) in our own facilities. To allow for statistical treatment, data were collected from three individual animals in each group (Gene Expression Omnibus accession no. GSE-4105).

Data Analysis

Raw data were collected and analyzed using Affymetrix Microarray Suite 5.0 (MAS) software. After the scanning, array images were assessed by eye to confirm scanner alignment and the absence of significant bubbles or scratches. 3′/5′ Ratios for GAPDH and β-actin were confirmed to be within acceptable limits. BioB spike controls were present on the chips, with BioC, BioD, and CreX also present in increasing intensity. When scaled to a target intensity of 1,500 (using Affymetrix MAS 5.0 array analysis software), scaling factors for all arrays were within acceptable limits, as were background values, Q-values, and mean intensities. Additional processing of data was performed using dChip software (14) and Data Mining Tool software (DMT, Affymetrix). Initial filtering of data was performed using DMT on absolute files generated from MAS. As an initial filter, *t*-test was utilized to identify differentially expressed genes between the sham vs. the I-R group ($n = 3$ replicates in each group). Genes that significantly ($P < 0.05$) changed (increased or decreased) in the I-R group compared with sham were selected. Next, for data visualization and clustering, genes initially filtered using the statistical (*t*-test) approach by DMT were subjected to hierarchical clustering using dChip (v1.3) software. The following major clusters of genes, which were different in the I-R group compared with sham group, were selected for further data processing: *1*) up- or downregulated only on *day 7* post-I-R, *2*) up- or downregulated only on *day 2* post-I-R, and *3*) up- or downregulated on both *days 2* and *7* post-I-R. To minimize the number of false positives, the selected genes, using clustering approach, were further subjected to comparison analysis using the dChip software with the use of the following criteria: *1*) *t*-test, $P < 0.05$; *2*) present call in all experimental (I-R) samples for upregulated genes; and *3*) present call in all baseline (sham) samples for downregulated genes. To handle the multiple-comparison issue in the context of microarray data, the empirical false discovery rate (FDR) was estimated by permutations (38). Gene lists with a median FDR <5% have been presented. The significant genes were functionally categorized, and the following three major categories of genes were identified and have been presented in tabular form: *1*) extracellular matrix, *2*) apoptosis, and *3*) inflammation. Functional categorization was performed using the following software/web resources: Gene Ontology Data Mining Tool (Affymetrix); Kyoto Encyclopedia of Genes and Genomes (KEGG); Database for Annotation, Visualization, and Integrated Discovery Verification (DAVID) (5), and LocusLink (Swiss-Prot) as described previously (30). Microarray data were verified using real-time PCR assay.

mRNA Quantitation

Tissue mRNA was quantified by real-time PCR assay using double-stranded DNA-binding dye SYBR Green-I as described previously (28). The primer sets used for the individual genes are listed in Supplemental Table S1 (available at the *Physiological Genomics* web site).[1]

Histology

Histochemistry. Formalin-fixed tissues were embedded in paraffin and sectioned (4 μm), followed by hematoxylin and eosin staining.

Immunostaining. The sections were stained with the following primary antibodies: mouse monoclonal antibodies to p21 (1:50; Pharmingen), anti-ED-1 (1:100; Serotec), anti-smooth muscle actin (1:1,000; Sigma), anti-desmin (1:100; Dako), and anti-active caspase-3 (1:200, Cell Signaling).

Laser Microdissection and Pressure Catapulting

Laser microdissection and pressure catapulting (LMPC) was performed using the Microlaser System from P.A.L.M. Microlaser Technologies (Bernreid, Germany). Rat hearts with experimental occlusions were isolated, frozen in optimum cutting temperature (OCT) compound, and then cut into 10-μm sections with the use of a cryomicrotome. The sections were placed on polyethylene napthalate (PEN) membrane glass slides (P.A.L.M. Microlaser Technologies) that had been RNasin (Ambion, Austin, TX) and UV treated, for cutting and catapulting as described by our group recently (11). Sections were stored at −80°C and then thawed at room temperature for 5–10 min before use. Sections were stained using hematoxylin QS and the infarct site identified as reported (11). Infarcted areas of the section stained blue, whereas noninfarcted areas stained purple. Matched area ($0.8–1.0 \times 10^6$ μm^2) of noninfarct and infarct area was captured in chaotropic RNA lysis solution as described (11).

RNA Extraction and Reverse Transcription

RNA was extracted from catapulted elements using the RNAqueous-Micro Kit from Ambion according to their laser capture microdissection (LCM) protocol. Elements from three sections of same animal were pooled and incubated at 42°C for 30 min for RNA isolation. Extracted RNA was DNase treated at 37°C for 30 min, and the resulting RNA solution was used in reverse transcription reactions.

Reverse transcription was carried out using the Full Spectrum RNA Amplification Kit from System Biosciences (SBI, Mountain View, CA) according to the manufacturer's instructions. Reactions were performed in 10-ml volumes containing RT buffer, primers, dNTPs, DTT, and RT. Reaction conditions included 4-min incubation at 70°C with primer and RNA alone followed by 5-min incubation at 25°C.

[1] The Supplemental Material for this article (Supplemental Tables S1–S7) is available online at **http://physiolgenomics.physiology.org/cgi/content/full/00013.2006/DC1**.

Transcription buffer, dNTPs, DTT, and RT were then added, and the resulting solution was incubated at 42°C for 50 min followed by 4 min at 70°C.

Total cDNA Amplification and mRNA Quantification

cDNA from reverse transcription reactions was amplified using the Full Spectrum RNA Amplification Kit from SBI. Each reaction solution contained PCR buffer, dNTPs, proprietary primers, and DNA polymerase. PCR cycling was done according to the manufacturer's instructions, except that the number of cycles was increased to 25. Cycling conditions included 95°C for 4 min and 68°C for 5 min followed by 95°C for 25 s, 58°C for 1 min, and 68°C for 1.5 min. Next, 25 cycles at 95°C for 25 s and 68°C for 1.5 min were carried out followed by a 2-min extension step at 68°C. Typically, 1 μl of this solution was used for real-time PCR. Real-time PCR assay was performed using double-stranded DNA-binding dye SYBR Green-I as described previously (28, 30).

Statistics

Data shown as bar graphs are means ± SD. Student's *t*-test or ANOVA was used to test significance of difference between means. $P < 0.05$ was interpreted as significant difference between means. For Fig. 8*D*, the simple χ^2-test was used. Statistics related to DNA microarray data processing are described above in *Data Analysis*.

RESULTS

The compensation for myocardial infarction by myocardial gene expression in the peri-infarct site is known to occur at an early phase after myocardial infarction, and myocardial dysfunction is thought to begin from adjacent to remote peri-infarcted myocardium during progressive cardiac remodeling (18). A survival model of left anterior descending coronary artery occlusion for 30 min followed by reperfusion in rats was employed to examine changes in the transcriptome of the I-R heart tissue. The loss of blood flow during occlusion was verified by laser Doppler flowmetry, and the infarct tissue was subjected to histological characterization. Masson trichrome staining of the infarct region revealed progressive receding of the myocyte line indicating the time course of infarction-induced loss of myocyte viability (Fig. 1*A*). Distinct changes were observed in *day 2*, which we refer to in this work as the early inflammatory phase. The histological changes in the peri-infarct site were progressive and continued until *day 7* (Fig. 1*A*) beyond which the changes were not as marked as a function of time (not shown). Thus we chose to compare findings from *day 2* with those from *day 7*, which we refer to in this work as the late inflammatory phase. Histological characterization of the late inflammatory phase revealed the

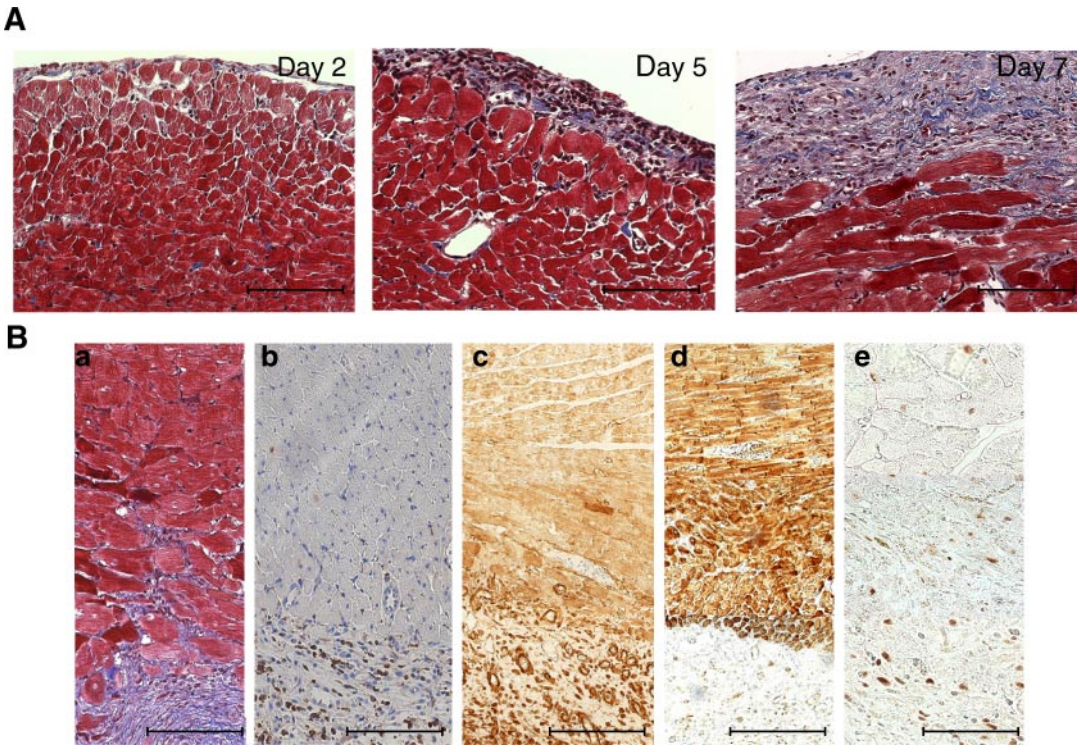

Fig. 1. Histological characterization of remodeling cardiac tissue used for genomic studies. Occlusion (30 min) of left anterior descending coronary artery was followed by reperfusion. Ischemia was documented by laser Doppler flow measure. On successful reperfusion, the thorax was closed, and negative thoracic pressure was reestablished for survival. Formalin-fixed paraffin sections from *day 7* postreperfusion heart were stained using the following. *A*: Masson trichrome procedure (*days 2*, *5*, and *7* postreperfusion). This procedure results in blue-black nuclei and blue collagen and cytoplasm; cardiac muscle fibers are stained red. *Ba*: Masson trichrome-stained *day 7* postreperfusion section showing the remodeling cardiac tissue. Next, immunostainings were performed to characterize the tissue illustrated in *Ba*. *Bb*: monocyte/macrophage (ED-1, brown): recognizes a single-chain glycoprotein of 110 kDa that is expressed predominantly on the lysosomal membrane of rat monocyte/macrophages. The antigen recognized by ED-1 (brown) in the rat is a homolog of human CD68. Blue (nuclei) is counterstaining with hematoxylin. *Bc*: α-smooth muscle antibody that recognizes α-isotype of smooth muscle actin (brown) present on myofibroblasts and smooth muscle and myoepithelial cells. *Bd*: desmin (brown): antibody recognizes skeletal, cardiac, and smooth muscle cells. *Be*: p21 (brown, nuclear stain): recognizes the p21/WAF1 protein, which is an important cell cycle regulatory protein. p21 inhibits cell cycle progression at both the G1 and G2 checkpoints. Scale bar = 100 μm.

receding myocyte line, which was cohabited by infiltrating macrophages (Fig. 1*B*, *a* and *b*). The peri-infarct site was also habited by the characteristic myofibroblasts, which are produced by the differentiation of resident cardiac fibroblasts. The myofibroblasts were identified as α-smooth muscle actin-positive (Fig. 1*Bc*) and desmin-negative cells (Fig. 1*Bd*). Consistent with our previous reports demonstrating that p21 plays a central role in triggering the differentiation of cardiac fibroblasts to myofibroblasts at the peri-infarct site of myocardial infarction, this cell cycle regulatory protein was detected at the peri-infarct site (Fig. 1*Be*).

The specific objective of this study was to identify changes in the I-R rat myocardial transcriptome in the early (*day 2*) and late (*day 7*) inflammatory phases of acute myocardial infarction. Identical tissue harvested from sham-operated rats subjected to the same surgical procedures, where the ligature was inserted in the heart but not tied, was used as control for comparison purposes. Three independent experiments were performed to enable appropriate statistical analyses. Figure 2 depicts the experiment design and data analysis approach, which are consistent with our previous reports (27, 30). Data processing was initially performed using MAS and DMT (v2.0) softwares. Additional data filtration was performed using dChip, employing the following specific criteria: *1*) *t*-test, $P < 0.05$ (median FDR <5%); *2*) present call in all I-R test samples for upregulated genes; and *3*) present call in all sham control samples for downregulated genes. This approach for data analysis identified 119 genes that were significantly and uniquely upregulated in *day 2*, 193 genes that were upregulated commonly in *days 2* and *7*, and 590 genes that were uniquely upregulated in *day 7* after I-R. Overall, fewer genes were downregulated by I-R. It was identified that 38 genes were downregulated significantly and uniquely in *day 2*, 216 genes were downregulated commonly in *days 2* and *7*, and 286 genes were uniquely downregulated in *day 7* (Fig. 2). Hierarchical cluster images of these candidate genes are illustrated in Fig. 3. A list of candidate genes of each category is provided as Supplement Materials (Supplemental Tables S2–S7). The candidate genes represented three major functional categories: extracellular matrix, apoptosis, and inflammation. The pattern of expression of genes representing these specific functional groups in the post-I-R remodeling heart is presented in Fig. 4. A complete list of all candidate genes belonging to the specific functional groups illustrated in Fig. 4 is presented in Tables 1–3.

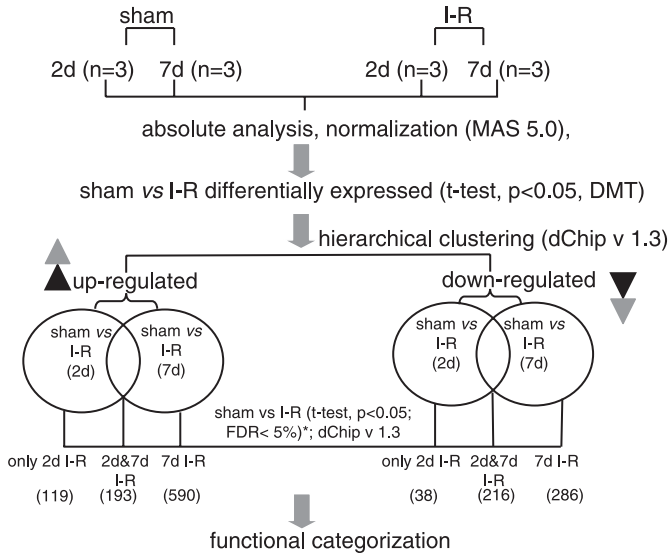

Fig. 2. Experimental design and data analysis scheme. GeneChip data analysis scheme used to identify differentially expressed genes from cardiac tissue harvested from rats subjected to ischemia (30 min) and reperfusion (I-R) for 2 days (2d) or 7 days (7d) compared with control tissue, i.e., rats that underwent sham surgery (sham). Data processing was initially performed using Microarray Suite 5.0 (MAS) and Data Mining Tool 2.0 (DMT) softwares. Additional data filtration was performed using dChip, employing the following specific criteria: *1*) *t*-test, $P < 0.05$ [median false discovery rate (FDR) <5%]; *2*) present call in all I-R test samples for upregulated genes; and *3*) present call in all sham control samples for downregulated genes. Details of software and other resources for data analysis are provided in MATERIALS AND METHODS.

To verify accuracy of the microarray analyses, four candidate genes were randomly selected from Supplemental Table S3 for real-time PCR analyses. The four genes were thrombospondin-4 (*TSBP4*), endothelial type gp91-phox gene (*Cybb*), follistatin-like (*Fstl*), and fibroblast activation protein (*FAP*). Quantitative real-time PCR analyses of the individual genes provided results that were consistent with microarray findings (Fig. 5). Next, we identified candidate genes from the three functional groups to verify whether the microarray analyses could be reproduced by quantitative real-time PCR. To expand on our microarray findings dealing with two time points, *days 2* and *7*, we examined tissues collected from *days 0*, *0.25*, *2*, *3*, *5*, and *7*. In the category of inflammation, the expression of interleukin-6 (IL-6) and IL-18 was investigated. Acute myocardial infarction resulted in upregulation of both of these cytokines. Significant induction of both IL-6 as well as IL-18 was noted in *day 2*, and the effect was more prominent in *day 3*. After *day 3*, the inducible response for both cytokines subsided (Fig. 6*A*). Myocardial healing response is characterized by the deposition of type I and III collagen (9, 18). The progression of response to acute myocardial infarction in the functional category of extracellular matrix was not akin to the inflammatory mediators. In contrast, genes encoding extracellular matrix proteins such as types I and III collagen were appreciably upregulated in *day 2,* and that response progressively grew stronger until *day 7* after I-R (Fig. 6*B*). Comparable response kinetics was exhibited by the candidate genes of the apoptosis category. Caspases-2, -3, and -8 were induced in response to acute infarction. For all three genes, the change was significant in *day 2* after I-R (Fig. 6*C*). The effect was more prominent in *day 7* after infarction, consistent with the observation for genes in the extracellular matrix category (Fig. 6*B*). There is mounting evidence that apoptosis is important in the pathogenesis of myocardial infarction. One of the key events in the process of apoptosis is activation of caspase-3 (43). Thus we chose to histologically evaluate the presence of caspase-3 protein in the myocardial tissue that was harvested 7 days after infarction. Compared with the myocardial tissue from the sham-operated rats, tissue collected from the infarct region stained heavily positive for the presence of active caspase-3 (Fig. 7). The LMPC technology has the unique ability to harvest spatially defined tissue that is typically not possible to collect while tissue in the infarct region is harvested surgically. Our laboratory (11) has recently standardized the application of this technology to examine the spatially resolved

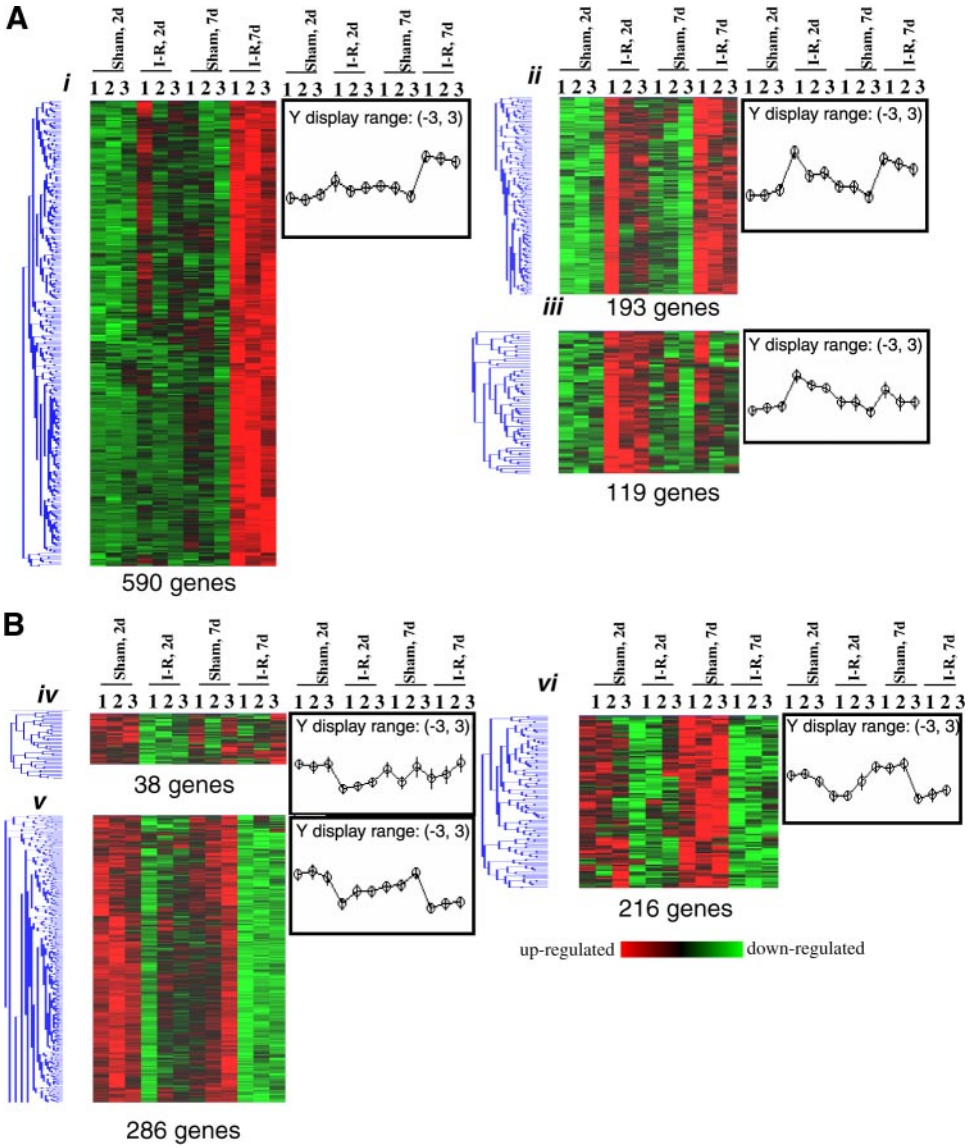

Fig. 3. Hierarchical cluster images illustrating remodeling-sensitive genes in cardiac tissue induced or downregulated after I-R. Specific clusters of genes showing an increase (*A*) or decrease (*B*) in expression after ischemia (30 min) and reperfusion (2d or 7d). Genes that were found significantly up- or downregulated in all replicates after I-R compared with sham-operated samples were selected. These select candidate genes were subjected to hierarchical clustering to identify clusters of genes that are induced/downregulated by I-R after 2d or 7d postreperfusion. *Cluster i*: cluster of genes upregulated specifically after 7d of reperfusion. *Cluster ii*: cluster of genes upregulated after both 2d and 7d of reperfusion. *Cluster iii*: cluster of genes upregulated specifically after 2d of reperfusion. *Cluster iv*: cluster of genes downregulated specifically after 2d of reperfusion. *Cluster v*: cluster of genes downregulated specifically after 7d of reperfusion. *Cluster vi*: cluster of genes downregulated after both 2d and 7d of reperfusion. Data shown are from 3 individual animals (*animals 1–3*). Graphs next to each image (at *right*) illustrate the average pattern of gene expression in the corresponding cluster. *Samples 1–3* in each group represent the replicates. Red-to-green gradation in color represents higher-to-lower expression signal.

biology of myocardial infarction. In this study, we applied LMPC to harvest infarct and adjacent noninfarct control tissues from microscopically defined regions in the rat myocardium. Our results show a very tight response demonstrating that type I collagen and type III collagen are potently induced in the infarct region but not in the tissue harvested beyond 500 μm away from the infarct site (Fig. 8). When compared, the LMPC approach was observed to generate tighter data with lower standard deviation than results derived from samples harvested by conventional surgical excision (Fig. 8).

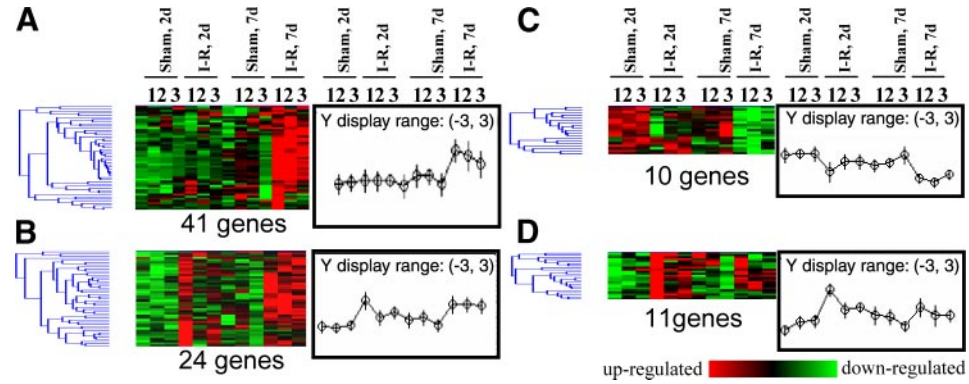

Fig. 4. Visualization of the expression pattern of candidate genes representing the specific functional groups in the remodeling myocardium after I-R. Genes from the following major functional groups were subjected to hierarchical clustering to visualize expression patterns of these genes after I-R. *A*: extracellular matrix. *B* and *C*: apoptosis. *D*: immune/inflammation. Graphs next to each image (at *right*) illustrate the average pattern of gene expression in the corresponding cluster. *Samples 1–3* in each group represent the replicates. Red-to-green gradation in color represents higher-to-lower expression signal.

Table 1. *Extracellular matrix protein-encoding genes upregulated after ischemia (30 min) and 7d reperfusion compared with 7d sham-operated animals*

Probe ID	Description	Symbol	Mean	SD
1368347_at	collagen, type V, alpha 3	Col5a3	15.9	5.2
1370265_at	arrestin, beta 2	Arrb2	3.5	1
1369955_at	collagen, type V, alpha 1	Col5a1	3.3	0.9
1369407_at	tumor necrosis factor receptor superfamily, member 11b (osteoprotegerin)	Tnfrsf11b	3.3	1
1370895_at	collagen, type V, alpha 2	Col5a2	3.1	0.4
1388138_at	thrombospondin 4	Thbs4	3	0.8
1373463_at	collagen, type V, alpha 2	Col5a2	2.9	0.2
1369968_at	pleiotrophin	Ptn	2.7	0.2
1387854_at	procollagen, type 1, alpha 2	Col1a2	2.7	0.4
1387854_at	procollagen, type 1, alpha 2	Col1a2	2.7	0.4
1370864_at	collagen, type 1, alpha 1	Col1a1	2.5	0.5
1367860_a_at	matrix metalloproteinase 14, membrane-inserted	Mmp14	2.5	0.4
1370155_at	procollagen, type 1, alpha 2	Col1a2	2.4	0.6
1367849_at	syndecan 1	Sdc1	2.4	0.4
1368838_at	tropomyosin 4	Tpm4	2.4	0.2
1370301_at	matrix metalloproteinase 2 (72 kDa type IV collagenase)	Mmp2	2.3	0.3
1370287_a_at	tropomyosin 1, alpha	Tpm1	2.3	0.6
1388116_at	collagen, type 1, alpha 1	Col1a1	2.2	0.4
1370847_at	F-spondin	VSGP	2.2	0.7
1367562_at	secreted acidic cysteine rich glycoprotein	Sparc	2.2	0.2
1388111_at	elastin	Eln	2.1	0.6
1367563_at	secreted acidic cysteine rich glycoprotein	Sparc	2.1	0.3
1368961_at	Matrix metalloproteinase 23	Mmp23	2	0.2
1375049_at	latent transforming growth factor beta binding protein 3	Ltbp3	1.9	0.2
1387886_at	proline arginine-rich end leucine-rich repeat protein	Prelp	1.9	0.2
1376099_at	collagen, type V, alpha 1	Col5a1	1.8	0.1
1370166_at	syndecan 2	Sdc2	1.7	0.2
1386940_at	tissue inhibitor of metalloproteinase 2	Timp2	1.7	0.1
1367574_at	vimentin	Vim	1.7	0.1
1370959_at	collagen, type III, alpha 1	Col3a1	1.6	0.3
1367749_at	lumican	Lum	1.6	0.1
1371518_at	nidogen (entactin)	Nid	1.6	0.1
1367807_at	procollagen-lysine, 2-oxoglutarate 5-dioxygenase (lysine hydroxylase, Ehlers-Danlos syndrome type VI)	Plod	1.6	0.3
1370167_at	syndecan 2	Sdc2	1.6	0.1
1370082_at	transforming growth factor, beta 1	Tgfb1	1.6	0.3
1371073_at	UDP-Gal:betaGlcNAc beta 1,4- galactosyltransferase, polypeptide 1	B4galt1	1.6	0.3
1374870_at	collagen, type XXVII, alpha 1	Col27a1	1.5	0.2
1367912_at	LanC (bacterial lantibiotic synthetase component C)-like 1	Ltbp1	1.5	0.2
1372877_at	procollagen-lysine, 2-oxoglutarate 5-dioxygenase 3	Plod3	1.5	0
1388698_at	extracellular matrix protein 1	Ecm1	1.4	0.2
1368989_at	tissue inhibitor of metalloproteinase 3	Timp3	1.2	0.1

Data presented indicate fold change (mean ± SD) in expression of ischemia (30 min) and reperfusion (7 day; 7d) compared with corresponding sham-operated control sample. Probe ID, Affymetrix probe identifications. Data correspond to Fig. 4, *cluster A*.

DISCUSSION

Myocardial infarction is associated with an inflammatory response. The inflammatory phase contributes to cardiac remodeling and eventual host outcome (8, 17, 26). Cytokine release is a hallmark of the early inflammatory phase. Our observation that IL-6 is induced in the early inflammatory phase is consistent with the prior observation that reperfusion rapidly induces IL-6 in the heart (12). It has been demonstrated recently that, following a preconditioning stimulus, IL-6 is obligatorily required for the activation of the JAK-STAT pathway, the ensuing upregulation of inducible nitric oxide synthase (iNOS) and cyclooxygenase-2 (COX-2), and the development of a cardioprotective phenotype (4). We noted that IL-18, a potent proinflammatory cytokine, was induced in the early inflammatory phase of reperfusion. Endogenous IL-18 has been reported to play a significant role in ischemia-reperfusion-induced human myocardial injury (24). Neutralization of IL-18 attenuates lipopolysaccharide-induced myocardial dysfunction (25). Furthermore, serum levels of IL-18 have been observed to be strong predictors of cardiac mortality in patients with coronary artery disease (37). The CCR2 chemokine receptor mediates leukocyte chemoattraction, which is involved in the pathogenesis of coronary heart disease. Our results show that CCR2 gene expression was induced in the early inflammatory phase. The CCR2 genotype is known to predispose patients for myocardial infarction before the age of 65 yr (19). Cybb (34) codes for gp91-phox, a component of NADPH oxidase. The expression of Cybb was induced in the early inflammatory phase, which is consistent with the previous finding that angiotensin AT(1) receptor activation results in NADPH oxidase gene expression in the ischemia-reperfused heart (20).

The extracellular matrix (ECM) is a key component in the remodeling process, and increases in collagen occur in the infarct area to replace necrotic myocytes and form a scar. The ECM is coupled to the cell through cell surface receptors,

Table 2. *Apoptosis genes up- and downregulated after ischemia (30 min) and 7d reperfusion compared with 7d sham-operated animals*

Probe ID	Description	Symbol	Mean	SD
	Upregulated			
1369262_at	caspase-8	Casp8	3.5	0.2
1369407_at	tumor necrosis factor receptor superfamily, member 11b (osteoprotegerin)	Tnfrsf11b	3.3	0.8
1387690_at	caspase 3	Casp3	2.6	0.7
1369198_at	apoptotic protease activating factor 1	Apaf1	2.3	0.4
1368305_at	caspase 6	Casp6	2.1	0.4
1390434_at	TNFRSF1A-associated via death domain	Tradd	1.9	0.1
1367856_at	glucose-6-phosphate dehydrogenase	G6pdx	1.8	0.2
1370112_at	phosphatase and tensin homolog	Pten	1.8	0.1
1368856_at	Janus kinase 2	Jak2	1.8	0.3
1367715_at	tumor necrosis factor receptor superfamily, member 1a	Tnfrsf1a	1.7	0.2
1387521_at	programmed cell death 4	Pdcd4	1.7	0.2
1389873_at	apoptosis-associated speck-like protein containing a CARD	Asc	1.7	0.1
1367890_at	caspase 2	Casp2	1.6	0.1
1387502_at	serine/threonine kinase 17b (apoptosis-inducing)	Stk17b	1.6	0.3
1390386_at	caspase 3	Casp3	1.6	0.1
1398286_at	cysteine-sulfinate decarboxylase	Csad	1.4	0.1
1371572_at	amyloid beta (A4) precursor protein	App	1.4	0.1
1368118_at	B-cell CLL/lymphoma 10	Bcl10	1.4	0.1
1369879_a_at	testis enhanced gene transcript	Tegt	1.3	0.0
1369084_a_at	Bcl-2-related ovarian killer protein	Bok	1.2	0.1
1387605_at	caspase 12	Casp12	1.2	0.0
1370226_at	cystatin B	Cstb	1.2	0.0
1367465_at	defender against cell death 1	Dad1	1.2	0.1
	Downregulated			
1372423_at	p53 apoptosis-associated target		−2.3	0.7
1372539_at	castration induced prostatic apoptosis-related protein 1	Cipar1	−1.7	0.3
1367641_at	superoxide dismutase 1	Sod1	−1.6	0.1
1370962_at	castration induced prostatic apoptosis-related protein 1	Cipar1	−1.5	0.1
1370321_at	programmed cell death 8 (apoptosis-inducing factor)	Pdcd8	−1.5	0.3
1369939_at	cytochrome c, somatic	Cycs	−1.5	0.1
1371638_at	Similar to zinc RING finger protein SAG, mRNA		−1.3	0.2
1370923_at	expressed in non-metastatic cells 6, protein (nucleoside diphosphate kinase)	Nme6	−1.2	0.1
1386973_a_at	mitogen activated protein kinase 8 interacting protein	Mapk8ip	−1.2	0.1
1369995_at	Fas-associated factor 1	Faf1	−1.2	0.0

Data presented indicate fold change (mean ± SD) in expression of ischemia (30 min) and reperfusion (7d) compared with corresponding sham-operated control sample. Data correspond to Fig. 4, *clusters B* and *C*.

primary of which are the integrins. In addition, the matrix metalloproteinases coordinate ECM turnover through degradation of ECM components. These processes ultimately, when favorable, pave the way for angiogenesis and cellular regeneration. Collagen is the major ECM protein in the heart and represents a crucial target for anti-remodeling and cardioprotective therapy (41). In the myocardium, collagen represents the most abundant structural protein of the connective tissue network. Its structural organization consists of a complex weave of collagen fibers that surrounds and interconnects myocytes, groups of myocytes, muscle fibers, and muscle bundles. In the current study, the largest functional group of

Table 3. *Immune/inflammatory genes upregulated after ischemia (30 min) and 2d reperfusion compared with 2d sham-operated animals*

Probe ID	Description	Symbol	Mean	SD
1387316_at	chemokine (C-X-C motif) ligand 1; gro	Gro1	7.9	3.7
1369191_at	interleukin 6	Il6	7.7	3.0
1367850_at	Fc receptor, IgG, low affinity III	Fcgr3	4.2	1.7
1398246_s_at	Fc receptor, IgG, low affinity III	Fcgr3	3.9	1.7
1367973_at	chemokine (C-C motif) ligand 2	Ccl2	3.6	1.0
1367581_a_at	secreted phosphoprotein 1	Spp1	3.5	1.4
1368683_at	oxidised low density lipoprotein (lectin-like) receptor 1	Olr1	3.4	0.8
1368490_at	CD14 antigen	Cd14	2.8	1.0
1390798_at	protein tyrosine phosphatase, receptor type, C	Ptprc	2.3	0.5
1369665_a_at	interleukin 18	Il18	2.0	0.2
1387742_at	chemokine receptor CCR2 gene	Ccr2	1.8	0.0

Data presented indicate fold change (mean ± SD) in expression of ischemia (30 min) and reperfusion (2d) compared with corresponding sham-operated control sample. Data correspond to Fig. 4, *cluster D*.

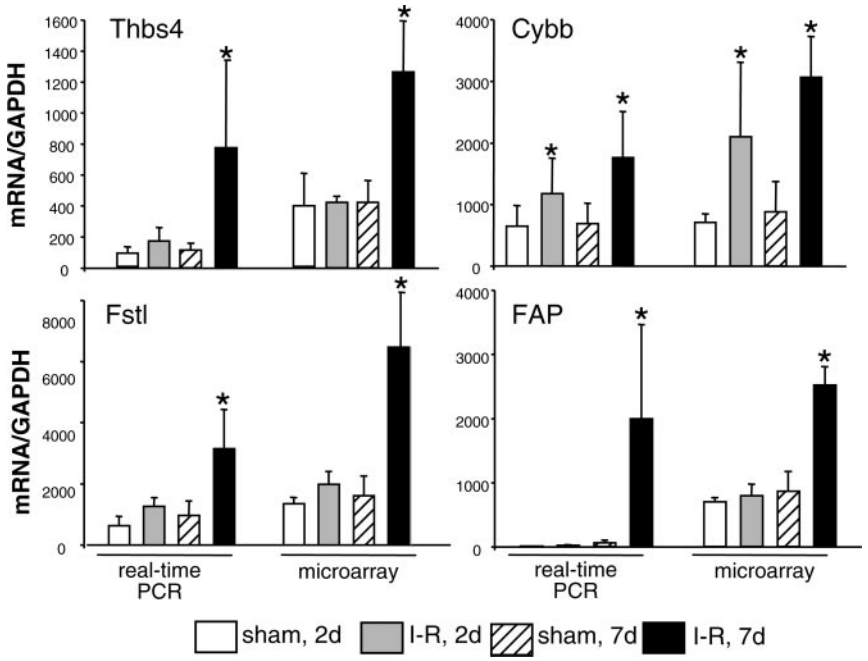

Fig. 5. Real-time PCR validation of GeneChip microarray expression analysis. Expression levels of selected genes identified using GeneChip analysis were independently determined using real-time PCR. For comparison, the real-time PCR data (normalized to GAPDH, a housekeeping gene) were proportionately adjusted to fit to the scale with GeneChip expression values (normalized using global scaling approach). *Thbs4*, thrombospondin-4; *Cybb*, endothelial type gp91-phox gene; *Fstl*, follistatin-like; *FAP*, fibroblast activation protein. Data represent means ± SD. $*P < 0.05$: significantly higher compared with the corresponding sham samples.

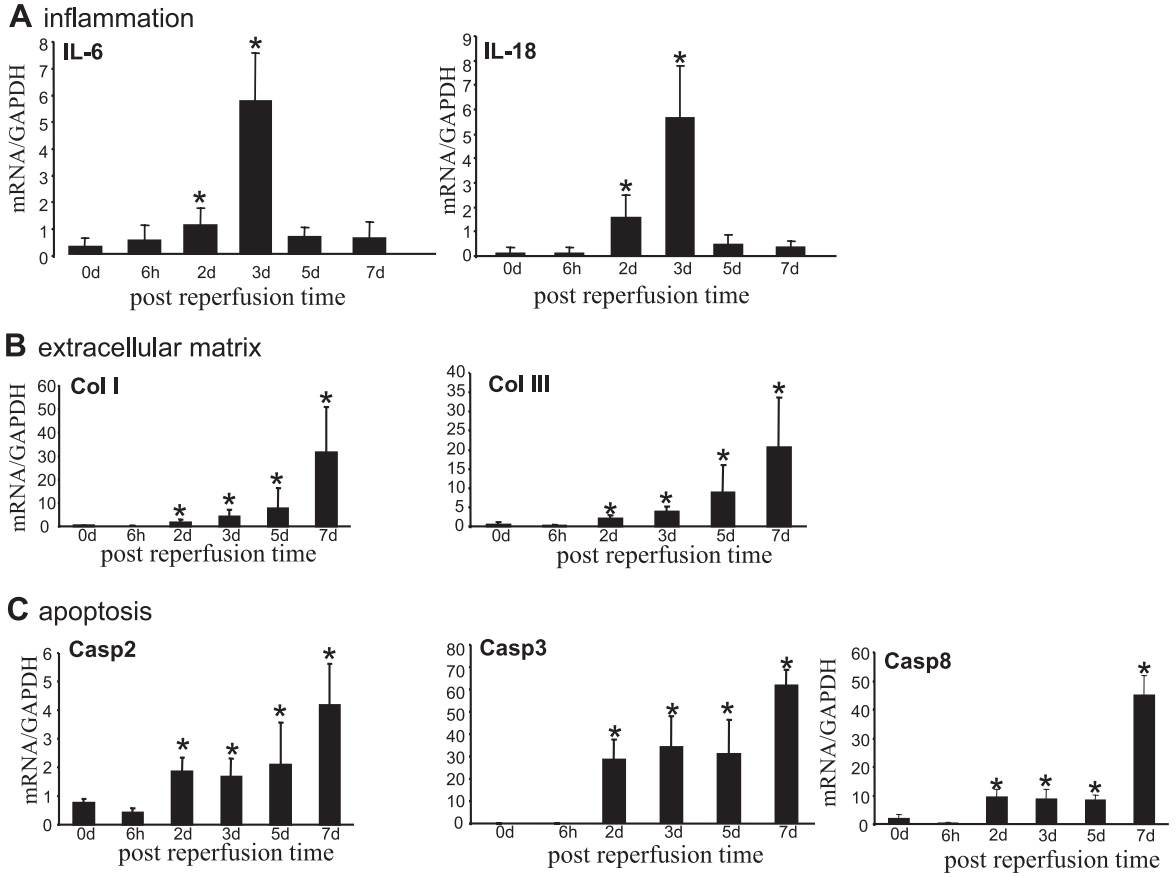

Fig. 6. Expression kinetics of representative genes from major functional groups as identified using microarray in a reperfused myocardium. Expression kinetics of selected genes in reperfused (6 h to 7d) myocardium after 30 min of ischemia. These genes belonged to 3 functional groups *A*: inflammation. *B*: extracellular matrix. *C*: apoptosis. Functional groups and representative genes were identified using the microarray approach. mRNA expression analysis was performed using real-time PCR. Real-time PCR data were normalized to GAPDH, a housekeeping gene. Casp, caspase; Col, collagen; IL, interleukin. Data are mean ± SD. *, $P < 0.05$ compared with day 0.

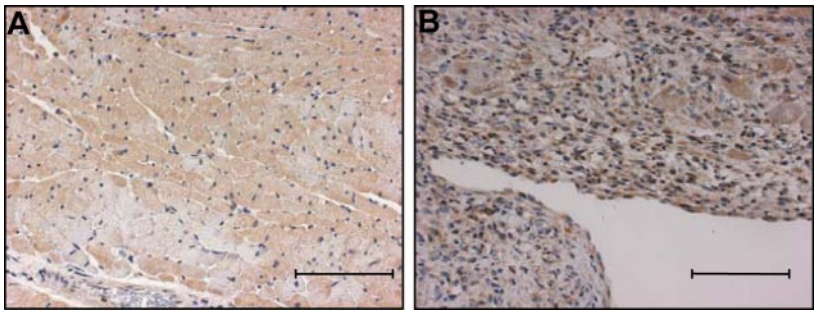

Fig. 7. Histological evaluation of expression of active caspase-3 in reperfused myocardium. Active caspase-3 expression in sham (*A*) vs. I-R (*B*) heart of rats harvested 7d after infarction. By use of the microarray approach, caspase-3 mRNA was identified to be upregulated after 7d of I-R. To verify the results at the protein expression level, immunostaining was performed using anti-active caspase-3 antibody (brown). Counterstaining was performed using hematoxylin (blue, nuclei). Scale bar = 100 μm.

genes observed to be induced in the late inflammatory phase was represented by those that encode proteins of the ECM. When findings from the microarray studies were expanded, including additional time points, it was observed that both collagen I and III were induced in the early phase, but the induction got progressively stronger from *day 2* to *day 7* after reperfusion. The expression of these two specific types of collagen is known to be induced by reperfusion of the heart (18). Wound healing begins with the proliferation of young fibroblasts positive for type I, III, and V collagens at the wound margin. Next, vascular granulation tissue grows into the injured myocardium followed by deposition of fibrous components immunoreactive with types I and III (9). Fibroblast activation protein-α (FAP) is a cell surface serine protease expressed at sites of tissue remodeling in embryonic development. FAP is not expressed by mature somatic tissues except activated melanocytes, tumor stroma, and fibroblasts in wound healing (13, 15). Our study suggests that FAP is induced in the remodeling phase of ischemia-reperfused heart. Thrombospondins are a family of extracellular calcium-binding proteins that are involved in cell proliferation, adhesion, and migration. Thrombospondin-4 binds specifically to both collagenous and noncollagenous ECM proteins via its COOH-terminal domains (16). Thrombospondin-4 is expressed by vascular cells and influences the vessel wall by modulating the proliferation of endothelial cells and smooth muscle cells (35). Recently, an elevated level of expression of thrombospondin-4 has been reported in scar tissue (21). Our results provide the first evidence demonstrating elevated expression of thrombospondin-4 in the late inflammatory phase. Polymorphic thrombospondin-4 gene has been identified to perturb calcium homeostasis (36) and contribute to the development of myocardial infarction in humans at any age (39).

Seven years ago it was observed that the pharmacological inhibitor of caspase ZVAD-fmk effectively reduces myocardial reperfusion injury (40). Ever since, interest in the significance of caspases in the infarcted myocardium has soared. The postinfarct treatment with caspase inhibitors improved left ventricular remodeling and dysfunction through inhibition of granulation tissue cell apoptosis (7). Caspases, which are the executioners of apoptosis, comprise two distinct classes, initiators and effectors. Although general structural features are shared between the initiator and the effector caspases, their activation, inhibition, and release of inhibition are differen-

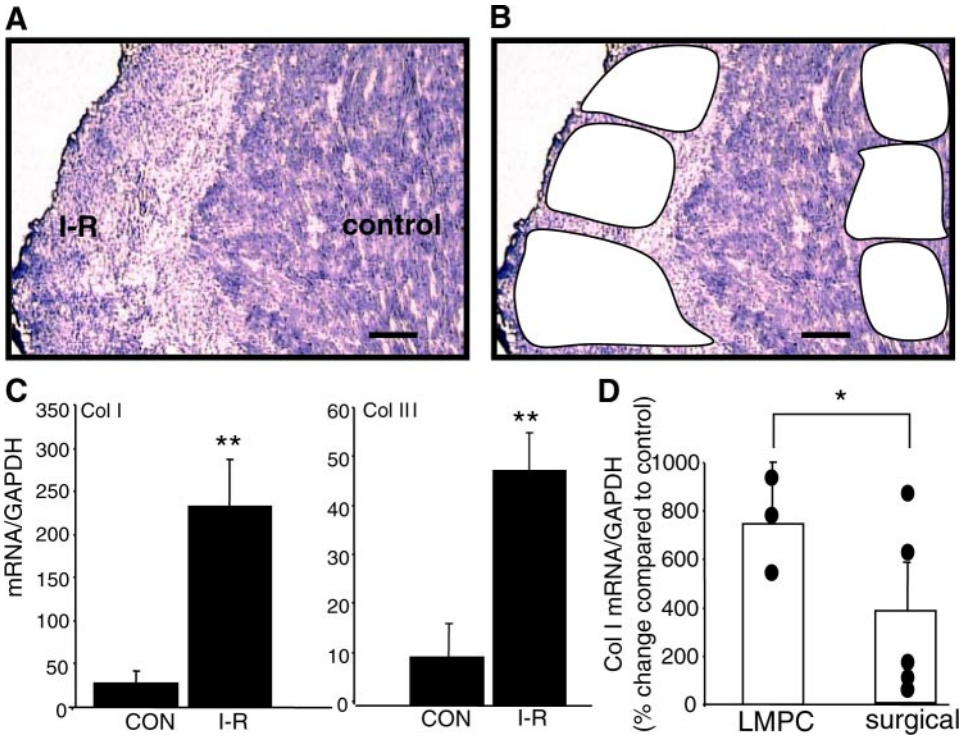

Fig. 8. mRNA expression analysis of histologically defined areas of I-R rat hearts using laser microdissection and pressure catapulting (LMPC). *A* and *B*: frozen sections (10 μm) from heart of rats subjected to ischemia (30 min) and reperfusion (7d) were stained with hematoxylin to histologically define infarct and control areas in the same microscopic field. *A*: representative stained frozen section showing distinct I-R and control regions. *B*: same section as shown in *A* after the elements from the I-R and control areas have been cut and captured. Scale bar = 100 μm. *C*: mRNA expression analysis of collagen I and collagen III from laser-captured I-R and control areas. mRNA analysis was performed using real-time PCR. Real-time PCR data were normalized to GAPDH, a housekeeping gene. Data are means ± SD ($n = 3$). $^{**}P < 0.005$ compared with control. *D*: comparison of collagen I mRNA expression analysis using conventional surgical tissue excision or LMPC techniques. mRNA analysis was performed on frozen section samples using real-time PCR. Data are presented as %change compared with corresponding control area. Data are shown as individual %change data points (as scatter plot) as well as means ± SD (as bar graph overlay). $^{*}P < 0.05$: simple χ^2-test demonstrated lower SD in LMPC compared with conventional surgical procedure.

tially regulated. Long-term caspase inhibition ameliorated apoptosis, reduced myocardial troponin I cleavage, protected left ventricular function, and attenuated remodeling in rats with myocardial infarction (2). Recent studies show that treatment with a caspase-3 inhibitor improves survival and prevents ventricular dilation and dysfunction after permanent coronary artery occlusion (1). In this study, we noted concurrent induction in the expression of caspases-2 (initiator), -3 (effector), and -8 (initiator). The induction for all three genes was more intense in the late inflammatory phase than in the early inflammatory phase. Our observation that active caspase-3 protein expression in the reperfused myocardium is high in the late inflammatory phase is consistent with the recent report demonstrating an elevated presence of activated caspase-3 in the infarcted human myocardium (43). Caspase-2 appears to be necessary for the onset of apoptosis triggered by several insults, including DNA damage and inflammation (42). Caspase-8 is required for killing induced by the death receptors Fas, tumor necrosis factor receptor-1, and death receptor-3. Moreover, caspase-8-deficient mice die in utero as a result of defective development of heart muscle and display fewer hematopoietic progenitor cells, suggesting that the FADD/caspase-8 pathway is absolutely required for the growth and development of myocardial cells (10). It is yet unknown whether such cytotrophic function of caspase-8 is implicated in postinfarction myocardial remodeling.

Taken together, this work presents the first evidence gained from the use of DNA microarrays to understand the molecular mechanisms implicated in the early and late inflammatory phases of the ischemia-reperfused heart. With the use of the high-density oligonucleotide microarray approach, an excess of 15,000 well-annotated full-length genes and ESTs were surveyed in the early and later inflammatory phases of acute myocardial infarction. Definite patterns of candidate genes emerged and are indicative of the functional responses underlying myocardial infarction. The reported findings represent a resource that may be utilized to develop testable hypotheses examining the fundamental mechanisms implicated in the reperfused myocardium.

GRANTS

This work was supported by National Heart, Lung, and Blood Institute Grant RO1-HL-073087 to C. K. Sen.

REFERENCES

1. **Balsam LB, Kofidis T, and Robbins RC.** Caspase-3 inhibition preserves myocardial geometry and long-term function after infarction. *J Surg Res* 124: 194–200, 2005.
2. **Chandrashekhar Y, Sen S, Anway R, Shuros A, and Anand I.** Long-term caspase inhibition ameliorates apoptosis, reduces myocardial troponin-I cleavage, protects left ventricular function, and attenuates remodeling in rats with myocardial infarction. *J Am Coll Cardiol* 43: 295–301, 2004.
3. **Cleutjens JP, Blankesteijn WM, Daemen MJ, and Smits JF.** The infarcted myocardium: simply dead tissue, or a lively target for therapeutic interventions. *Cardiovasc Res* 44: 232–241, 1999.
4. **Dawn B, Xuan YT, Guo Y, Rezazadeh A, Stein AB, Hunt G, Wu WJ, Tan W, and Bolli R.** IL-6 plays an obligatory role in late preconditioning via JAK-STAT signaling and upregulation of iNOS and COX-2. *Cardiovasc Res* 64: 61–71, 2004.
5. **Dennis G Jr, Sherman BT, Hosack DA, Yang J, Gao W, Lane HC, and Lempicki RA.** DAVID: Database for Annotation, Visualization, and Integrated Discovery. *Genome Biol* 4: P3, 2003.
6. **Gidh-Jain M, Huang B, Jain P, Gick G, and El-Sherif N.** Alterations in cardiac gene expression during ventricular remodeling following experimental myocardial infarction. *J Mol Cell Cardiol* 30: 627–637, 1998.
7. **Hayakawa K, Takemura G, Kanoh M, Li Y, Koda M, Kawase Y, Maruyama R, Okada H, Minatoguchi S, Fujiwara T, and Fujiwara H.** Inhibition of granulation tissue cell apoptosis during the subacute stage of myocardial infarction improves cardiac remodeling and dysfunction at the chronic stage. *Circulation* 108: 104–109, 2003.
8. **Jefferson BK and Topol EJ.** Molecular mechanisms of myocardial infarction. *Curr Probl Cardiol* 30: 333–374, 2005.
9. **Kawahara E, Mukai A, Oda Y, Nakanishi I, and Iwa T.** Left ventriculotomy of the heart: tissue repair and localization of collagen types I, II, III, IV, V, VI and fibronectin. *Virchows Arch A Pathol Anat Histopathol* 417: 229–236, 1990.
10. **Kruidering M and Evan GI.** Caspase-8 in apoptosis: the beginning of "the end"? *IUBMB Life* 50: 85–90, 2000.
11. **Kuhn DE, Roy S, Radtke J, Gupta S, and Sen CK.** Laser microdissection and pressure catapulting technique to study gene expression in the reoxygenated myocardium. *Am J Physiol Heart Circ Physiol* 290: H2625–H2632, 2006.
12. **Kukielka GL, Youker KA, Michael LH, Kumar AG, Ballantyne CM, Smith CW, and Entman ML.** Role of early reperfusion in the induction of adhesion molecules and cytokines in previously ischemic myocardium. *Mol Cell Biochem* 147: 5–12, 1995.
13. **Levy MT, McCaughan GW, Abbott CA, Park JE, Cunningham AM, Muller E, Rettig WJ, and Gorrell MD.** Fibroblast activation protein: a cell surface dipeptidyl peptidase and gelatinase expressed by stellate cells at the tissue remodelling interface in human cirrhosis. *Hepatology* 29: 1768–1778, 1999.
14. **Li C and Wong WH.** Model-based analysis of oligonucleotide arrays: expression index computation and outlier detection. *Proc Natl Acad Sci USA* 98: 31–36, 2001.
15. **Mathew S, Scanlan MJ, Mohan Raj BK, Murty VV, Garin-Chesa P, Old LJ, Rettig WJ, and Chaganti RS.** The gene for fibroblast activation protein alpha (FAP), a putative cell surface-bound serine protease expressed in cancer stroma and wound healing, maps to chromosome band 2q23. *Genomics* 25: 335–337, 1995.
16. **Narouz-Ott L, Maurer P, Nitsche DP, Smyth N, and Paulsson M.** Thrombospondin-4 binds specifically to both collagenous and non-collagenous extracellular matrix proteins via its C-terminal domains. *J Biol Chem* 275: 37110–37117, 2000.
17. **Nian M, Lee P, Khaper N, and Liu P.** Inflammatory cytokines and postmyocardial infarction remodeling. *Circ Res* 94: 1543–1553, 2004.
18. **Omura T, Yoshiyama M, Takeuchi K, Hanatani A, Kim S, Yoshida K, Izumi Y, Iwao H, and Yoshikawa J.** Differences in time course of myocardial mRNA expression in non-infarcted myocardium after myocardial infarction. *Basic Res Cardiol* 95: 316–323, 2000.
19. **Ortlepp JR, Vesper K, Mevissen V, Schmitz F, Janssens U, Franke A, Hanrath P, Weber C, Zerres K, and Hoffmann R.** Chemokine receptor (CCR2) genotype is associated with myocardial infarction and heart failure in patients under 65 years of age. *J Mol Med* 81: 363–367, 2003.
20. **Oudot A, Vergely C, Ecarnot-Laubriet A, and Rochette L.** Angiotensin II activates NADPH oxidase in isolated rat hearts subjected to ischaemia-reperfusion. *Eur J Pharmacol* 462: 145–154, 2003.
21. **Paddock HN, Schultz GS, Baker HV, Varela JC, Beierle EA, Moldawer LL, and Mozingo DW.** Analysis of gene expression patterns in human postburn hypertrophic scars. *J Burn Care Rehabil* 24: 371–377, 2003.
22. **Pfeffer MA and Braunwald E.** Ventricular remodeling after myocardial infarction. Experimental observations and clinical implications. *Circulation* 81: 1161–1172, 1990.
23. **Pfeffer MA, Pfeffer JM, Fishbein MC, Fletcher PJ, Spadaro J, Kloner RA, and Braunwald E.** Myocardial infarct size and ventricular function in rats. *Circ Res* 44: 503–512, 1979.
24. **Pomerantz BJ, Reznikov LL, Harken AH, and Dinarello CA.** Inhibition of caspase 1 reduces human myocardial ischemic dysfunction via inhibition of IL-18 and IL-1beta. *Proc Natl Acad Sci USA* 98: 2871–2876, 2001.
25. **Raeburn CD, Dinarello CA, Zimmerman MA, Calkins CM, Pomerantz BJ, McIntyre RC Jr, Harken AH, and Meng X.** Neutralization of IL-18 attenuates lipopolysaccharide-induced myocardial dysfunction. *Am J Physiol Heart Circ Physiol* 283: H650–H657, 2002.

26. **Ren G, Dewald O, and Frangogiannis NG.** Inflammatory mechanisms in myocardial infarction. *Curr Drug Targets Inflamm Allergy* 2: 242–256, 2003.
27. **Roy S, Khanna S, Bentley K, Beffrey P, and Sen CK.** Functional genomics: high-density oligonucleotide arrays. *Methods Enzymol* 353: 487–497, 2002.
28. **Roy S, Khanna S, Bickerstaff AA, Subramanian SV, Atalay M, Bierl M, Pendyala S, Levy D, Sharma N, Venojarvi M, Strauch A, Orosz CG, and Sen CK.** Oxygen sensing by primary cardiac fibroblasts: a key role of p21(Waf1/Cip1/Sdi1). *Circ Res* 92: 264–271, 2003.
29. **Roy S, Khanna S, and Sen CK.** Perceived hyperoxia: oxygen-regulated signal transduction pathways in the heart. *Methods Enzymol* 381: 133–139, 2004.
30. **Roy S, Khanna S, Wallace WA, Lappalainen J, Rink C, Cardounel AJ, Zweier JL, and Sen CK.** Characterization of perceived hyperoxia in isolated primary cardiac fibroblasts and in the reoxygenated heart. *J Biol Chem* 278: 47129–47135, 2003.
31. **Roy S, Lado BH, Khanna S, and Sen CK.** Vitamin E sensitive genes in the developing rat fetal brain: a high-density oligonucleotide microarray analysis. *FEBS Lett* 530: 17–23, 2002.
32. **Sen CK, Khanna S, and Roy S.** Perceived hyperoxia: oxygen-induced remodeling of the reoxygenated heart. *Cardiovasc Res*. In press.
33. **Stanton LW, Garrard LJ, Damm D, Garrick BL, Lam A, Kapoun AM, Zheng Q, Protter AA, Schreiner GF, and White RT.** Altered patterns of gene expression in response to myocardial infarction. *Circ Res* 86: 939–945, 2000.
34. **Stasia MJ.** Gene symbol: CYBB. Disease: X-linked chronic granulomatous disease. *Hum Genet* 116: 236, 2005.
35. **Stenina OI, Desai SY, Krukovets I, Kight K, Janigro D, Topol EJ, and Plow EF.** Thrombospondin-4 and its variants: expression and differential effects on endothelial cells. *Circulation* 108: 1514–1519, 2003.
36. **Stenina OI, Ustinov V, Krukovets I, Marinic T, Topol EJ, and Plow EF.** Polymorphisms A387P in thrombospondin-4 and N700S in thrombospondin-1 perturb calcium binding sites. *FASEB J* 19: 1893–1895, 2005.
37. **Tiret L, Godefroy T, Lubos E, Nicaud V, Tregouet DA, Barbaux S, Schnabel R, Bickel C, Espinola-Klein C, Poirier O, Perret C, Munzel T, Rupprecht HJ, Lackner K, Cambien F, and Blankenberg S.** Genetic analysis of the interleukin-18 system highlights the role of the interleukin-18 gene in cardiovascular disease. *Circulation* 112: 643–650, 2005.
38. **Tusher VG, Tibshirani R, and Chu G.** Significance analysis of microarrays applied to the ionizing radiation response. *Proc Natl Acad Sci USA* 98: 5116–5121, 2001.
39. **Wessel J, Topol EJ, Ji M, Meyer J, and McCarthy JJ.** Replication of the association between the thrombospondin-4 A387P polymorphism and myocardial infarction. *Am Heart J* 147: 905–909, 2004.
40. **Yaoita H, Ogawa K, Maehara K, and Maruyama Y.** Attenuation of ischemia/reperfusion injury in rats by a caspase inhibitor. *Circulation* 97: 276–281, 1998.
41. **Zannad F and Radauceanu A.** Effect of MR blockade on collagen formation and cardiovascular disease with a specific emphasis on heart failure. *Heart Fail Rev* 10: 71–78, 2005.
42. **Zhivotovsky B and Orrenius S.** Caspase-2 function in response to DNA damage. *Biochem Biophys Res Commun* 331: 859–867, 2005.
43. **Zidar N, Dolenc-Strazar Z, Jeruc J, and Stajer D.** Immunohistochemical expression of activated caspase-3 in human myocardial infarction. *Virchows Arch*: 1–5, 2005.